Cold flow characteristics of a novel bluff body hydrogen burner

Christoph Meraner[a,*], Tian Li[a], Mario Ditaranto[b], Terese Løvås[a]

[a] *Department of Energy and Process Engineering, Faculty of Engineering, NTNU Norwegian University of Science and Technology, Trondheim, Norway*
[b] *SINTEF Energy Research, Trondheim, Norway*

Abstract

The cold flow characteristics of a novel partial premixed bluff body (PPBB) low NO_x burner, capable of operating with hydrogen as well as methane-hydrogen blends, were investigated numerically. The PPBB burner features a frustum shaped conical bluff body generating a flame stabilizing recirculation zone. Fuel is partially premixed via jets in an accelerating cross-flow. Steady-state and transient non-reacting simulations using five different turbulence models, i.e. standard k-ϵ, realizable k-ϵ, shear stress transport (SST) k-ω, stress-blended eddy simulation (SBES) and large eddy simulation (LES), were conducted. The simulations were validated against particle image velocimetry (PIV) measurements of an unconfined non-reacting flow. All turbulent models were able to predict the recirculation zone length in good agreement with the experimental data. However, only scale resolving simulations could reproduce velocity magnitudes with sufficient accuracy. Time averaged and instantaneous results from the scale resolving simulation were

*Corresponding author
Email address: christoph.meraner@ntnu.no (Christoph Meraner)

analysed in order to investigate flow characteristics that are special about the PPBB burner design and of relevance for the combustion process. Two different burner configurations were studied and their effects on the flow field were examined. The recirculation zone volume as well as the entrainment into the wall jet around the bluff body were found to correlate with the elevation of the bluff body relative to the burner throat. Both of these parameters are expected to have a strong impact on the overall NO_x emission, since the near burner region is typically one of the main contributors to the NO_x formation.
Keywords: bluff body flow, low NO_x burner, CFD simulations, turbulence modelling, stress-blended eddy simulation, conical wall jet

1. Introduction

Combustion of hydrogen and hydrogen-rich synthetic gaseous fuels, such as syngas have received increased attention in the context of climate change and the urgent need for alternative fuels [1, 2, 3]. The use of syngas is particularly attractive when obtained by gasification of coal, waste or CO_2-neutral biomass feedstock. In case of steam gasification, it is possible to combine the process with a subsequent water-gas shift reaction, in which CO and H_2O are converted to H_2 and CO_2. The CO_2 can then be captured and stored. This combined process is referred to as pre-combustion carbon capture and storage (CCS). Benefits of pre-combustion CCS are the maximisation of the hydrogen level and the high relative concentration of the carbon species as CO_2 [4, 5]. Although the combustion of hydrogen in air emits theoretically only water, the high reactivity and elevated combustion temperature generate harmful and regulated nitrogen oxides (NO_x), that to date, no commercial burner can mitigate easily. Hence, transitioning from natural gas to hydrogen and hydrogen-rich combustion comprises a trade-off between reduced CO_2 emissions and increased NO_x emissions. In order to mitigate this undesired effect, low NO_x combustion concepts need to be developed, while keeping the required fuel flexibility in mind.

Different techniques have been established in the industry to reduce NO_x emissions from combustion processes. They can be categorized into four groups: pre-treatment, combustion modification, process modification (such as the modification of a gas turbine cycle [6]) and post-treatment [7]. A key benefit of syngas is its wide flexibility in fuel sources [8]. However, this and in particular different processing techniques imply a significant variation in relative composition of syngas [9, 10], which makes pre-treatment challenging. Most post-treatment methods on the other hand are relatively simple to implement, but they represent expensive add-on costs and are not benefiting the combustion process in any way [7]. The U.S. Environmental Protection Agency (EPA) provides an overview on the total effective NO_x reduction and the cost effectiveness of different control techniques [11]. The report concludes that low NO_x and ultra low NO_x burner on its own have the best cost effectiveness. While the lowest NO_x levels are achieved by a combination of low NO_x burners and selective catalytic reduction (SCR). Hence, there is a strong incentive to develop low NO_x burners for both standalone as well as combined applications.

Low NO_x burners can utilize different design features to minimize NO_x emissions. A discussion on several of these designs can for example be found in previous studies [1, 9]. However, for the development of low NO_x burners that can cope with variable fuel compositions and potentially high hydrogen concentration special care needs to be taken, especially of combustion stability. Hydrogen has a unique impact on the behaviour of fuel mixtures due to its significantly different transport properties and flame speed compared to other gaseous fuels [12]. Several studies have investigated the non-linear dependence of flame properties (e.g. flashback and lean blowout) on the hydrogen concentration [13, 14, 15]. Due to the wider flammability limits, low levels of hydrogen can extend the lean stability limits of burners [16]. However, higher levels of hydrogen decrease the stability range, as a result of the increased probability of flashbacks [13].

One of the most common designs for low NO_x gas burners is the premixed swirl burner. However, such burners are particularly prone to flashbacks at elevated hydrogen concentrations [17]. This is attributed to the premixing as well as the potential for combustion induced vortex breakdown (CIVB), which is related to the interaction of heat release and swirling flows [9, 18, 19]. In order to avoid these issues associated with premixed swirl burners, Spangelo et al. [20] developed and patented a novel partially premixed bluff body burner (PPBB burner) that aims to ensure stable combustion with low NO_x emissions across a wide range of hydrogen concentrations. The PPBB burner combines advanced mixing techniques with burner generated internal flue gas recirculation (IFGR), which is sometimes referred to as furnace gas recirculation. A more detailed description of the PPBB burner design features is given in section 2.

The PPBB burner has been investigated experimentally by Dutka et al. and has proven good emission performance at laboratory scale [21, 22]. However, the scalability of the system is not yet well understood. For a successful scaling of the burner to larger dimensions and practical applications it is necessary to obtain a deeper understanding of the burner flow characteristics and their changes at different scales. The conducted experimental campaigns have been limited to the analysis of the flow field in a defined 2D observation window downstream of the bluff body as well as global emission measurements for NO_x, O_2, CO and CO_2. One of the main objectives for the present study is therefore to extend the investigated parameters by applying computational fluid dynamic (CFD) simulations, which allow to get a broader picture of the flow characteristics. In the context of scaling the main requirement for CFD simulations is to adequately represent qualitative trends depending on the burner scale. However, simulating the entire complexity of hydrogen combustion in a challenging geometry, including chemical reactions, different species properties, radiation, etc. involves the use of several submodels in addition to solving the equations describing the turbulent flow field. Hence, it is ambiguous to quantify uncertainties attributed to individual submodels. Thus the complexity of such a simulation needs to be increased gradually. The scope of the present study was therefore limited to the modelling of the non reacting air flow, which dominates the burner aerodynamics. This approach allows a clear distinction between aerodynamic and combustion driven effects and builds a solid foundation for future investigations with increased model complexity and focus on different burner scales.

By excluding any chemical reactions from the flow it was possible to validate the turbulence model without the additional uncertainty that derives from the various submodels related to combustion. Different turbulence models were employed to identify the model requirements for an adequate description of the major burner characteristics. The applied turbulence models ranged from two equation RANS models, that model the whole turbulence spectrum, to LES simulations which resolve the large scales and model only the subgrid scales. A comprehensive comparison was made between well-known models such as the standard k-ϵ model and a novel stress-blended eddy simulation (SBES) model, which has been recently developed by the ANSYS® turbulence team [23, 24]. The SBES model represents a compromise between RANS and LES models. It resolves large scale turbulence only away from walls, while modelling the entire turbulence spectrum close to walls. A more detailed descriptions of the underlying numerics of the SBES model is provided in section 3. All conducted numerical simulations were validated against the measurements obtained by Dutka et al. [25, 26].

2. The PPBB burner

The PPBB burner is designed for furnaces and boilers, operating at low pressure. Its main components consist of a cylindrical lance, holding a conical frustum shaped bluff body mounted concentrically, within a cylindrical housing (see figure 1). The bluff buddy is partially retracted into the housing forming a converging segment in which the narrowest cross-section is referred to as burner throat. The bluff body holds eight primary fuel ports located upstream of the throat and four secondary fuel ports downstream of the throat. Note that the secondary fuel ports are offset from the primary fuel ports in tangential direction (i.e., they are located ”between” primary fuel ports). The laboratory scale burner operates at a nominal thermal load of

10 kW.

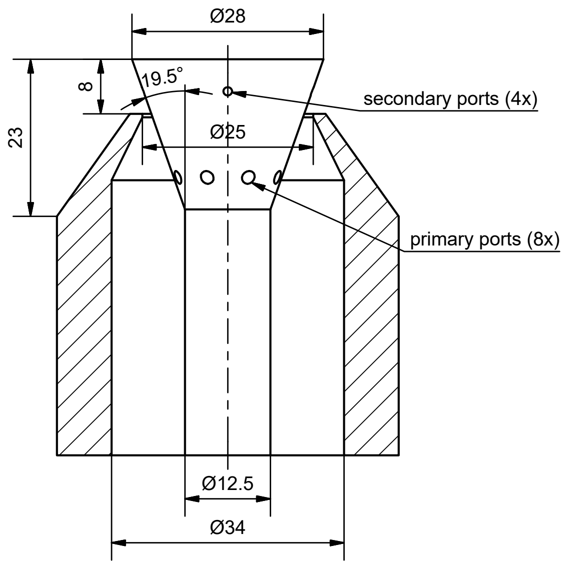

Figure 1: Schematic of the PPBB burner (dimensions in mm).

Figure 2 illustrates the flow pattern generated by the PPBB burner. Air is provided through the annular duct formed by the lance and burner housing. The majority of fuel (70% of the total fuel mass flow) is provided through the primary fuel ports, located in the converging section of the burner, where it is mixed in the accelerating cross flow. This configuration allows for rapid mixing and avoids ignitable unburned mixture in low axial velocity regions, which potentially could lead to flashback in the core flow, a well known phenomena as described by Plee and Mellor [27]. Furthermore, the accelerating flow ensures thin boundary layers, preventing flame back propagation within the boundary layer itself. Flashback in the boundary layer has been extensively studied for conventional fuels such as pure methane [28, 29, 30] and more recently also for syngas with different hydrogen concentrations

[31, 32, 33]. Lieuwen et al. [9] concludes: "Keeping the boundary layers as thin as possible is an essential design criterion for syngas burners [...]".

The remaining 30% fuel mass flow is provided trough the secondary fuel ports downstream of the throat, which creates small regions of enriched mixture downstream of the bluff body trailing edge. Dutka et al. [25] investigated the effect of different secondary fuel fractions on flame stability and NO_x emissions. The study showed that the impact of secondary fuel on the burner performance is correlating strongly to the hydrogen concentration in the fuel as well as the lance height (i.e., elevation of the bluff body trailing edge in relation to the throat). The burner configurations assessed in the present study (i.e., 8 mm and 16 mm lance height) have been found to provide optimal emission performance for the PPBB burner operating with pure hydrogen and pure methane respectively [25].

Bluff body flame stabilization has been studied extensively, even though it is less common than swirl flame stabilization. Recent studies of conical bluff body stabilized flames have been conducted by Kariuki et al. [34, 35] (unconfined), Andreini et al. [36] (confined) and Dawson et al. [37] (confined and unconfined). A unique feature of the PPBB burner is, however, the elevated position of the bluff body with regards to the burner throat (see figure 1). Since the bluff body is not fully immersed, it is possible to realize a minimum housing diameter that is smaller than the bluff body diameter itself. This leads to a blockage ratio larger than 100%, where the blockage ratio is defined as the ratio of bluff body cross section to minimum housing cross section. The PPBB can therefore by characterized by a conical wall jet flow around the bluff body. Only limited studies have investigated conical wall jets [38, 39, 40]. Research activities are mainly focusing on plane, radial or cylindrical wall jets. The latter two can be seen as limiting cases of a conical wall jet for a half-angle of 90° and 0° respectively. The plane wall jet is in turn the limiting case for a cylindrical wall jet with infinite large radius. Sharma [38] found that the spread angle as well as the shape of the velocity profiles are independent of the cone half-angle. The decrease of the maximal jet velocity in flow direction is on the other hand depending on the half-angle. The velocity decreases faster with an increased half-angle.

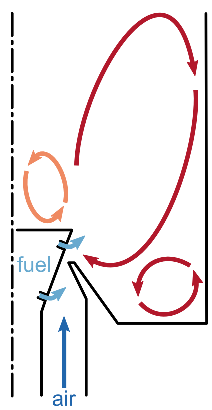

Figure 2: Illustration of the PPBB burner flow pattern. Primary and secondary fuel ports are drawn in the same plane for illustration purpose.

The elevated lance position is a crucial and unique feature of the PPBB burner for NO_x emission control and fuel flexibility. It allows entrainment of internal recirculated flue gas into the conical wall jet upstream of the flame anchor point (see figure 2). Recirculation of flue gas internally increases the overall efficiency compared to external flue gas recirculation. Understanding and controlling the amount of recirculated flue gas is therefore highly important.

3. Numerical methods

The PPBB burner was simulated using steady-state Reynolds averaged (RANS) as well as transient scale resolving simulations employing ANSYS® Academic Fluent, Release 18.1. All simulations were based on the assumption of incompressible flow. The density was calculated based on the incompressible ideal gas law based on the operational pressure (i.e., atmospheric pressure for the PPBB burner). The highest velocities in the PPBB burner (realized in the burner throat) are significant lower then the speed of sound in air (i.e., Ma $\sim$ 0.15) which justifies this assumption. Gravitational forces were neglected.

The governing equations for the conservation of mass and momentum as well as the transport equations for the respective turbulence model were discretised based on the finite volume method. A second order upwind scheme [41] was used to discretise the convective terms of the RANS transport equations and a less dissipative bounded central difference scheme [42] was used for the scale resolving simulations. The diffusive terms were discretised with a second order central difference scheme. The transient simulations were realized by use of a bounded second order implicit scheme. The SIMPLEC algorithm [43] was applied for the pressure-velocity coupling in all steady state simulations while a fractional-step method (FSM) [44, 45, 46, 47] in conjunction with a non-iterative time advancement (NITA) was used for all transient simulations. The transport equations were solved using a point implicit (Gauss-Seidel) linear equation solver in conjunction with an algebraic multigrid method [48]. ANSYS® Academic Fluent, Release 18.1. employs a co-located scheme (i.e., pressure and velocity are both stored at the cell centres) which requires a pressure interpolation scheme to retrieve the pressure at the cell faces. A second order central difference scheme was used for the pressure interpolation. Gradients and derivatives were evaluated employing a cell-based method (i.e., least squares cell based gradient evaluation), solving the coefficient matrix by use of the Gram-Schmidt process [49].

All transient simulations were conducted on the full domain as shown in figure 3. Different domain sizes were tested to ensure that the boundaries were located sufficiently far from the burner. A quarter of the domain was used for all RANS simulations, such that only two primary and one secondary fuel port were included in the domain. The RANS simulations were realised using periodic boundary conditions (see figure 3b). The applied boundary conditions are shown in figure 3. A constant velocity, normal to the boundary, of 4.0 m/s for the 8 mm lance height and 4.2 m/s for the 16 mm lance height configuration was imposed at the velocity inlet, corresponding to the experimental setup [25]. The turbulence kinetic energy at the velocity inlet was calculated based on the turbulence intensity which was assumed to be 5% and a hydraulic diameter of 4 mm (corresponding to the largest hole diameter in the perforated plate used to stabilize the flow, see figure 3.2 b in [50]) was used to estimate the corresponding turbulence dissipation rate. Atmospheric pressure was imposed at all open boundaries together with a turbulent intensity of 5% and a turbulent viscosity ratio of 10 which were used to calculate the corresponding turbulence kinetic energy and dissipation rate. Flow entering the domain at the pressure outlet or flow leaving the domain at the pressure inlet was defined as backflow. The direction of the backflow was set to be normal to the boundary for both of the pressure boundaries. A sensitivity study with varying turbulent boundary conditions showed negligible effect on the main flow features.

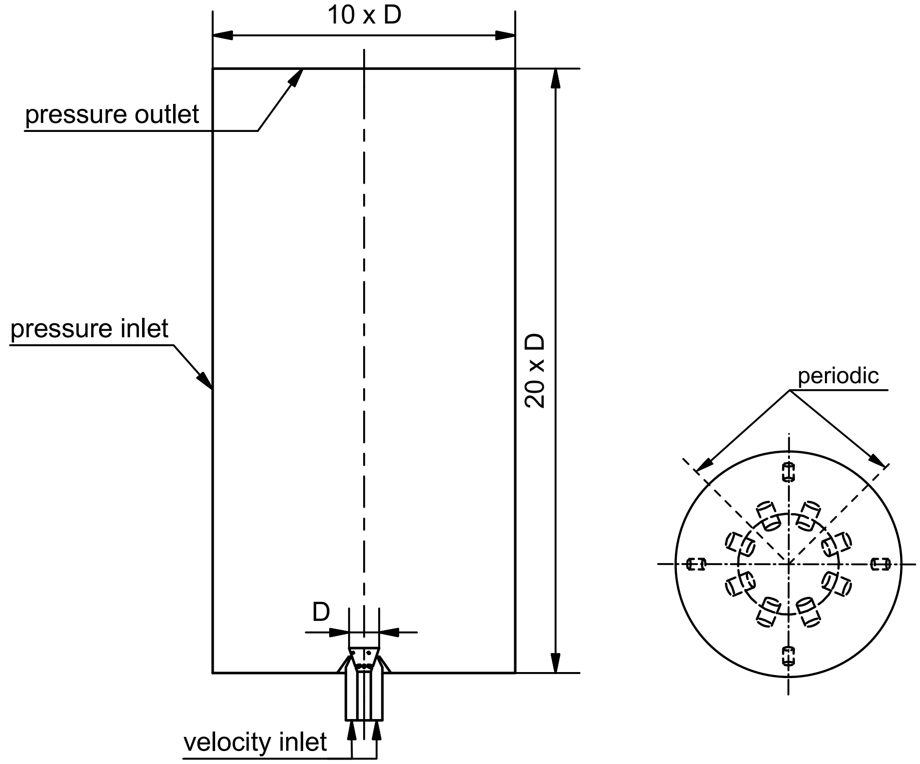

(a) Side view of the computational domain at 8 mm lance height.

(b) Top view of the burner lance indicating the location of the periodic boundaries (dashed lines).

Figure 3: Dimensions of the computational domain and boundary conditions. All unspecified boundaries are set to no-slip wall.

Five different turbulence modelling approaches, i.e. standard k-ϵ [51], realizable k-ϵ [52], SST k-ω [53], SBES [23, 24] and LES with the WALE subgrid model [54], were investigated. All RANS models were applied in steady state as well as unsteady (URANS) mode. The LES simulations have been performed on the same numerical grid as the SBES simulations, hence under resolving the wall boundary layers. The SBES model represents a new paradigm of turbulence modelling. A further description of the model is therefore provided in the following paragraph. Descriptions of the other turbulence models can be found in the corresponding literature.

The SBES model is a RANS-LES hybrid model capable of switching rapidly from an underlying RANS model to an algebraic LES model. The SBES formulation is based on the the shielded detached eddy simulation (SDES) model, which aims to prevent grid-induced separation (one of the main shortcomings of detached eddy simulation models) by introducing an asymptotic shielding function, f_s and an alternative grid scale. The strong shielding of f_s allows the SBES formulation to blend existing RANS and LES models on the stress-level:

$$\tau_{ij}^{SBES} = f_s \cdot \tau_{ij}^{RANS} + (1 - f_s) \cdot \tau_{ij}^{LES} \tag{1}$$

where τ_{ij}^{RANS} is the RANS part and τ_{ij}^{LES} the LES part of the modelled stress tensor. If both, the RANS and the LES model, are eddy-viscosity models the formulation simplifies to:

$$\nu_t^{SBES} = f_s \cdot \nu_t^{RANS} + (1 - f_s) \cdot \nu_t^{LES}. \tag{2}$$

The SBES formulation is in this sense not a new turbulence model, but rather a novel way to blend two existing models. This approach allows therefore to combine different RANS and LES models. The SBES model has, to the authors knowledge, not yet been employed for studying advanced burner configurations such as the PPBB burner. The SBES simulations of the PPBB burner were conducted by blending the SST-k-ω model in the RANS region with the WALE subgrid model in the LES region.

The PPBB burner represents a complex geometry due to the arrangement of its several fuel ports. It is challenging to represent such a geometry with a structured hexahedral mesh. Several alternative mesh topologies (i.e., tetrahedral, polyhedral, cut-cell and tetrahedral/hexahedral hybrid mesh) were tested in this study. Hybrid meshes utilize the flexibility of unstructured meshes in complex areas of the fluid domain while maintaining the higher accuracy of structured hexahedral meshes in simpler regions. However, they are not as easily generated as fully unstructured meshes and extra attention has to be given to the transition region between different mesh topologies (i.e., from tetrahedral/polyhedral to hexahedral cells). Hybrid meshes are therefore not ideal for the future up scaling of the PPBB burner, which will require the generation of multiple different meshes. Cut-cell meshes on the other hand can be generated using highly automated algorithms. They are characterized by predominantly high quality hexahedral cells. However, this comes at the cost of a few cells adjacent to the geometry with very high skewness. These low quality cells led to slow convergence of the PPBB burner simulations. Both tetrahedral and polyhedral meshes show a more uniformly distributed mesh quality and can easily adapt to complex geometry. Polyhedral meshes achieve the same accuracy as tetrahedral meshes at lower computational costs since they typically result in a significant lower total cell count than tetrahedral meshes. An unstructured polyhedral mesh with prism inflation layers at the walls was therefore found to be the most suited mesh topology for simulating the PPBB burner (see figure 4).

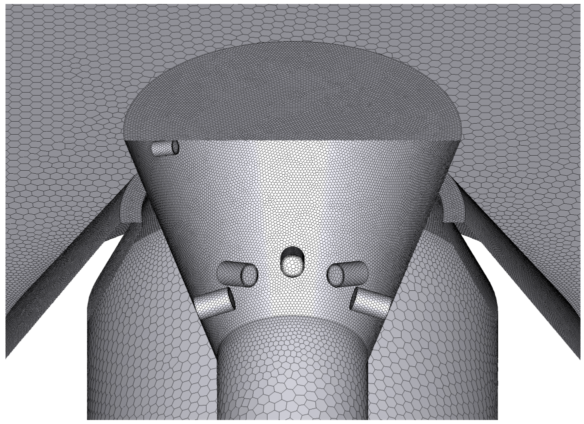

Figure 4: Half section view of the polyhedral surface mesh.

The mesh resolution was optimized for various flow regions by prescribing a size field (i.e., location specific maximum cell sizes). An example of such a size field can be seen in figure 5. A better representation of the transition between different cell size regions can be seen in figure 4. The growth rate in cell size was restricted to a maximum of 10% to ensure smooth transitions. However, initial scale resolving simulations indicated that the relatively narrow refinement shown in figure 5 had a noticeable effect on the flow field for the 8 mm lance height simulation. The refinement of the free shear layer and recirculation zone was therefore extended to a cylindrical region with a diameter of approximately two bluff body diameters and a height of 1.5 bluff body diameters for the scale resolving simulation of the 8 mm lance height. Mesh sensitivity simulations with different cell counts ranging from 2.9 M to 8.2 M cells were conducted. The final scale resolving simulations were realised with 4.0 M cells for the 16 mm configuration and 5.2 M cells for the 8 mm configuration. Boundary layer regions were resolved with values for the dimensionless wall distance (y^+) close to unity. The warped-face gradient correction was employed to improve gradient accuracy for non planar cell faces.

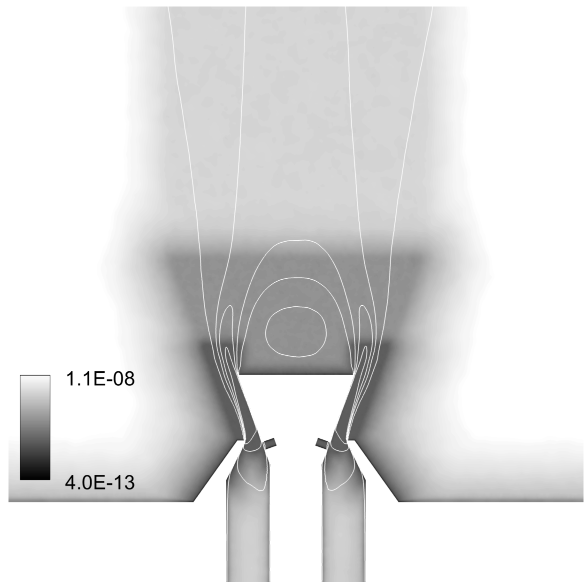

Figure 5: Cell volume with overlaid mean axial velocity iso-lines from the scale resolving 16 mm lance height simulation. Note an exponential colour scale is used for better readability.

4. Results

The results of the CFD based analysis are presented in three sections: Reynolds averaged simulations (4.1), scale resolving simulations (4.2) and the effect of different lance configurations (4.3). The first two sections are dealing with the validation of the applied CFD models, while the last one focuses on the alteration of the PPBB burner operational mode and its effect on the flow field characteristics, especially in regions that have not been accessible to PIV measurements.

4.1. Reynolds averaged simulations

Axial velocity profiles along the burner centreline were obtained from RANS and URANS simulations using different turbulence models. A comparison of these profiles to PIV data acquired by Dutka et al. [25] is shown in figure 6a and figure 6b respectively. All RANS simulations were able to predict the recirculation zone length. However, none of the applied models were capable to capture the velocity magnitudes of the flow field with a reasonable accuracy. All models were showing the same trend of over predicting velocities, especially within the recirculation zone. The SST k-ω model deviates most from the experimental data as seen in figure 6a. However, it performed better than the k-ϵ models in capturing the velocity decay in the developed jet region downstream of the recirculation zone. Neither the standard, nor the realizable k-ϵ model predicted the velocity decay correctly. The standard k-ϵ model was the only model that captured the maximal axial velocity downstream of the recirculation zone.

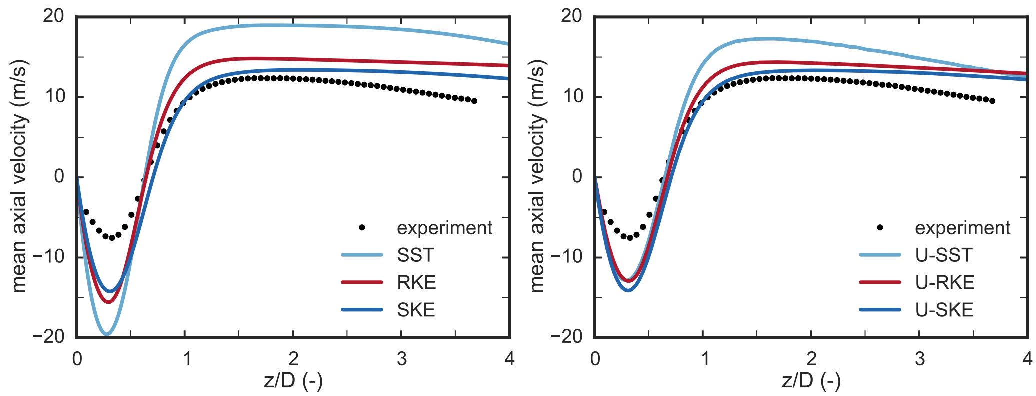

(a) RANS mode

(b) URANS mode

Figure 6: Mean axial velocity along the burner centreline for 8 mm lance height. Solid lines: standard k-ϵ (SKE), realizable k-ϵ (RKE) and SST k-ω (SST) simulations; dots: PIV measurement. Spacial coordinates are normalized by the bluff body diameter (D).

All three turbulence models were tested in URANS mode. The flow variables were, depending on individual simulations, sampled over a time period of 1.5 to 2 seconds, after an initial build-up time of 0.2 to 0.5 seconds. The resulting time averaged axial velocity profiles along the burner centreline are shown in figure 6b. Switching to URANS mode did improve the performance of the SST k-ω model considerably. Both k-ϵ models performed comparable to the RANS simulations, with a slight improvement of the realizable k-ϵ model. The high dissipation of the standard k-ϵ model prohibited the development of unsteady flow structures.

The normalized recirculating mass flow rate is given in table 1, along with the normalized dimensions of the recirculation zone. Typically the recirculating mass flow rate is normalized by the mass flow rate at the trailing edge of the bluff body as suggested by Taylor and Whitelaw [55]. Since this region was not captured by the PIV measurement, the inlet mass flow was used to normalize the recirculating mass flow rate. The recirculating mass flow rate measured by PIV was estimated based on the numerical integration of the axial velocity profile along the radius at the centre of the recirculation zone[1]. All applied turbulence models were able to reproduce the recirculation zone dimensions. However, they severely over predicted the recirculating mass flow rate. The SST k-ω model in URANS mode led to the best results, but still over predicted the recirculating mass flow rate by a factor of 2-3.

Table 1: Recirculation zone length (L) and width (W) normalized by the bluff body diameter (D) and normalized recirculation mass flow rate ($\frac{\dot{m}_r}{\dot{m}}$) predicted by the two equation turbulence models.

		$\frac{L}{D}$ (-)	$\frac{W}{D}$ (-)	$\frac{\dot{m}_r}{\dot{m}}$ (-)
	experiment	0.64	0.70	0.36
RANS	SST k-ω	0.63	0.75	1.26
RANS	realizable k-ϵ	0.64	0.75	1.15
RANS	standard k-ϵ	0.71	0.74	1.12
URANS	SST k-ω	0.65	0.80	0.82
URANS	realizable k-ϵ	0.67	0.80	1.08
URANS	standard k-ϵ	0.71	0.78	0.97

[1]The centre of the recirtculation zone was defined by the axial coordinate of the highest recirculation velocity on the burner centreline.

4.2. Scale resolving simulations

An accurate description of velocity magnitudes and hence residence time and recirculating mass flow rate in the recirculation zone is crucial for assessing combustion emissions. Scale resolved simulations were conducted, as the investigated RANS turbulence models performed poorly in this regard. The complex geometry of the PPBB burner, especially in hydrogen configuration (i.e., lance height of 8 mm) with large velocities in the narrow (1.32 mm) throat, is computational demanding for scale resolving simulations. The burner was therefore initially simulated in methane configuration (i.e., lance height of 16 mm). This configuration allowed a finer spatial and temporal resolution at lower numerical costs due to the wider throat opening and lower flow velocities. Moreover, the variation of the lance height made a qualitative assessment of its impact on the flow field accessible. The effect of varying the lance height on the flow field (i.e., change of air entrainment and recirculation zone length) is expected to be similar in the non-reacting and reacting flow configuration, even though absolute values will be different for these two scenarios. Experimental observations made by Dutka et al. [25] support this assumption.

4.2.1. Lance height 16 mm

Figure 7a shows the comparison of the mean axial velocity measured experimentally (left) and the mean axial velocity simulated using the SBES turbulence model (right). The velocity field of the SBES simulations was in good agreement with the PIV measurements. The simulation displayed slightly lower velocities in the centre of the flow and higher velocities in the shear layer flow. Note that the velocity field measured by PIV appears distorted close to the boarders of the contour plot. This is attributed to the limited number neighbouring interrogation windows at the boarders. The symmetry axis of the measured flow field is furthermore tilted by approximately 4° (see figure 7b). This was likely related to the difficulty of achieving perfect symmetry in an experimental set-up. Asymmetry can be caused by uneven air supply or centring inaccuracies of the lance. Small deviations in the alignment of lance and housing axis have a strong influence on the symmetry of the throat width due to the relatively large distance between the lance mounting point and the throat. Besides, flow field with recirculation are inherently hydrodynamically unstable.

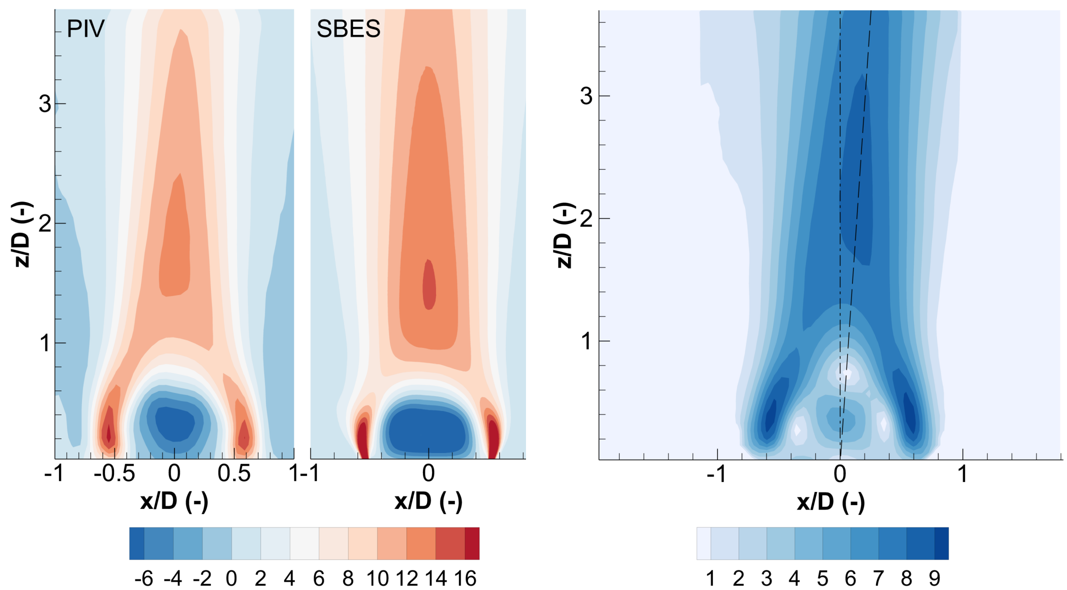

(a) mean axial velocity (m/s)

(b) mean two dimensional velocity magnitude (m/s)

Figure 7: a) Mean axial velocity from PIV measurement (left) and SBES simulation (right). b) Measured two dimensional mean velocity magnitude. The flow symmetry axis (dashed line) is tilted by $\sim 4^\circ$ from the burner centreline (dash doted).

Figure 8 shows the instantaneous visualisation of the iso-surface of the Q-criterion (which defines turbulent eddies as regions where the irrotational straining is small compared to the vorticity [56]) coloured by the SBES blending function. It can bee seen that the SBES model was able to shift quickly to LES mode (blue) outside the wall boundaries while structures close to the wall are in RANS mode (red). The model resolved small three-dimensional turbulent structures, which are visible in the recirculation zone.

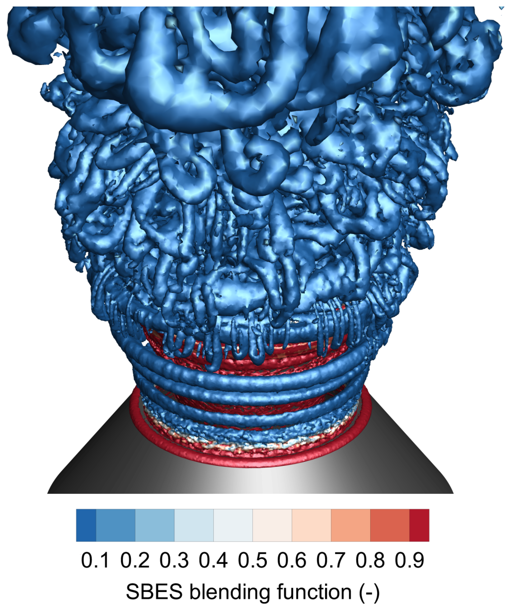

Figure 8: Q-criterion (10^4 s^{-2}) iso-surface coloured by the SBES blending function (where a value of 1 means RANS and a value of 0 means LES mode) from the 16 mm lance height simulation.

In figure 9 the velocity was corrected for the tilt of the flow field. The dots show the velocity along the symmetry axis of the flow, while the diamonds show the uncorrected velocity along the centreline of the burner. It is not possible to identify or correct for tilting of the flow field outside of the 2D plane covered by the PIV measurement. Hence, the observed tilt in the xz-plane is indicating the failure margin that can be expected for alignment deviations in the experimental set-up. However, the impact of it is less noticeable closer to the bluff body and can be neglected within the recirculation zone. The SBES and LES simulations, using the WALE subgrid model, showed almost identical results along the burner centreline (see figure 9). Both were in good agreement with the experimental data. The velocity magnitude were slightly under predicted by both modelling approaches. The difference between measured and simulated recirculating mass flow rate as well as recirculation zone length were below 10% for both simulations (see table 2).

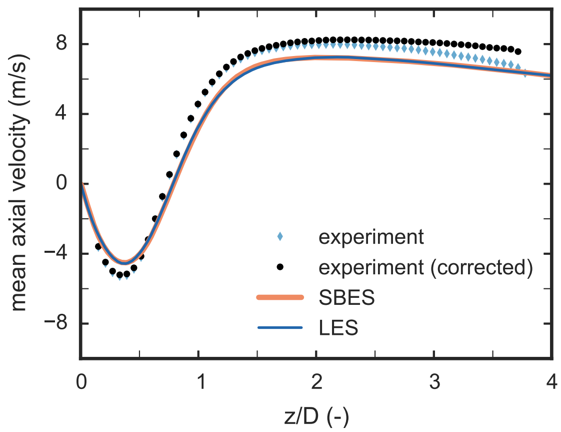

Figure 9: Mean axial velocity at 16 mm lance height. Bold red line: SBES simulation; blue line: LES simulation; diamonds: PIV measurement along burner centreline; dots: PIV measurement adjusted for $\sim 4°$ tilt of the mean flow field (see figure 7b).

Table 2: Size of recirculation zone and recirculation mass flow rate for 16 mm lance height.

	$\frac{L}{D}$ (-)	$\frac{W}{D}$ (-)	$\frac{\dot{m}_r}{\dot{m}}$ (-)
PIV	0.73	0.71	0.26
SBES	0.79	0.81	0.28
LES	0.78	0.86	0.27

4.2.2. Lance height 8 mm

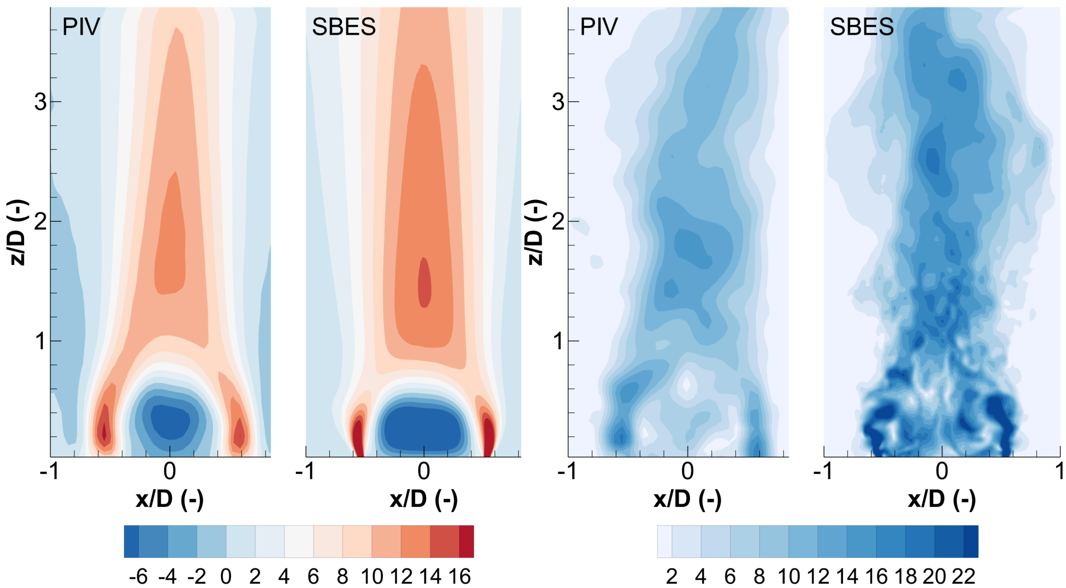

(a) mean axial velocity (m/s)

(b) instantaneous two dimensional velocity magnitude (m/s)

Figure 10: Comparison of mean and instantaneous velocity fields from PIV (left in the sub-figures) and SBES simulation (right in the sub-figures)

The measured flow field for 8 mm lance height did not display the same tilted symmetry axis as previous seen for the 16 mm lance height case (see figure 10b left), even though some asymmetry attributed to the experimental set up was still apparent. Comparing instantaneous flow fields from PIV and SBES simulations (see figure 10a) shows the higher resolution in the CFD simulation which allows to visualize smaller turbulent structures. The SBES simulation and the LES simulation, using the WALE subgrid model, produced very similar results. Figure 11 shows a comparison between these two models and experimental data as well as data from the SST k-ω model in URANS mode. The scale resolving simulation were able to capture the recirculation zone length as well as the velocity decay in the developed jet region reasonable well. The velocity magnitude were over predicted by the scale resolving simulations and the shape of the recirculation zone appeared not as spherical as in the PIV measurements. This was also reflected in the recirculating mass flow rate, which was significantly over predicted by the scale resolving simulations (see table 3).

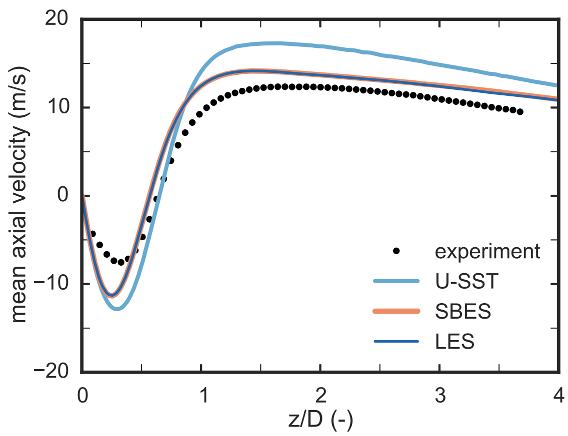

Figure 11: Mean axial velocity at 8 mm lance height. Light blue line: URANS SST k-ω simulation; bold red line: SBES simulation; thin dark blue line: LES simulation; dots: PIV measurement.

Table 3: Size of recirculation zone and recirculation mass flow rate for 8 mm lance height.

	$\frac{L}{D}$ (-)	$\frac{W}{D}$ (-)	$\frac{\dot{m}_r}{\dot{m}}$ (-)
PIV	0.64	0.70	0.36
SBES	0.57	0.80	1.56
LES	0.57	0.80	1.35

4.3. Effect of different lance configurations

Varying the lance height to adapt the PPBB burner to different fuel compositions affects the opening of the throat, the length of the wall jet region and the relative position of the fuel ports to the housing which leads to a different momentum ratio of the jet in cross flow configuration of the fuel injection. Extending the lance height increases the length of the recirculation zone and decreases the recirculating mass flow rate. This effect was observed in both the experiments and scale resolving simulations. The smaller throat opening of the 8 mm configuration led to higher velocities in the free shear layer downstream of the bluff body even thought the air mass flow rate was slightly lower than that for the 16 mm configuration (see figure 12). The simulation of the 16 mm configuration under predicted the shear layer spread compared to the experimental data more than the simulation of the 8 mm configuration. However, the centre region of the flow was better reproduced in the 16 mm simulation.

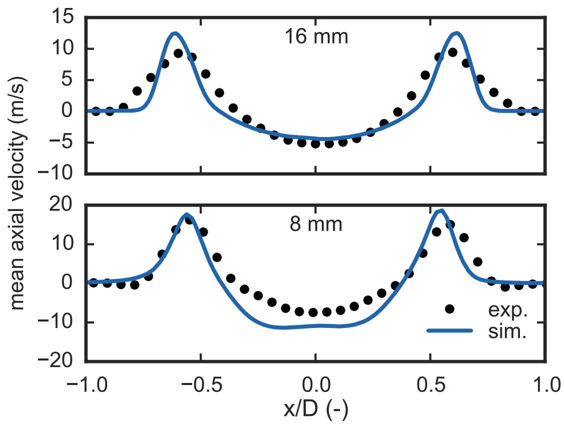

Figure 12: Axial velocity profile along the burner x-axis obtained from PIV (dots) and LES simulations (solid line) at 0.3 bluff body diameters downstream of the bluff body trailing edge.

The region close to the bluff body wall was not accessible by the conducted PIV measurements. Time averaged data of the wall jet was therefore obtained from the LES simulations for 8 mm and 16 mm lance height to give new insight into the flow structure in this region. Figure 13 shows a set of normalized velocity profiles close to the wall at various positions in flow direction between throat and bluff body trailing edge. The velocity is decomposed into a component parallel to the wall (u_w) and a component perpendicular to the wall (v_w). The velocity is normalized by the maximum velocity in flow direction (u_{max}) and the wall coordinate (y_w) is normalized by the wall jet half-width ($y_{1/2}$) which is the cross-stream distance corresponding to half of the maximum velocity. The coordinate in flow direction (x_w) is normalized by minimum throat width (δ_{throat}). The velocity in the throat (x_w/δ_{throat}=0) contains a noticeable velocity component towards the bluff body wall caused by the converging burner housing. This component decays in flow direction.

However, the velocity profiles do not reach self-similarity. A similar trend can be seen in figure 14a for the simulation of 8 mm lance height. However, at x_w/δ_{throat}=3.1 the profiles start to collapse in the outer layer as seen in figure 14b.

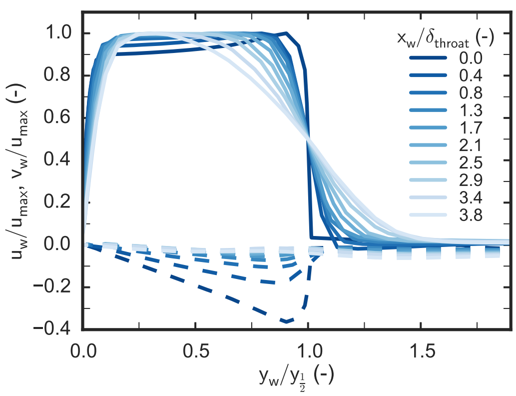

Figure 13: Normalized velocity profiles in the wall jet region obtained from LES simulations of 16 mm lance height. (solid lines) velocity component parallel to wall, (dashed lines) velocity component perpendicular to the wall.

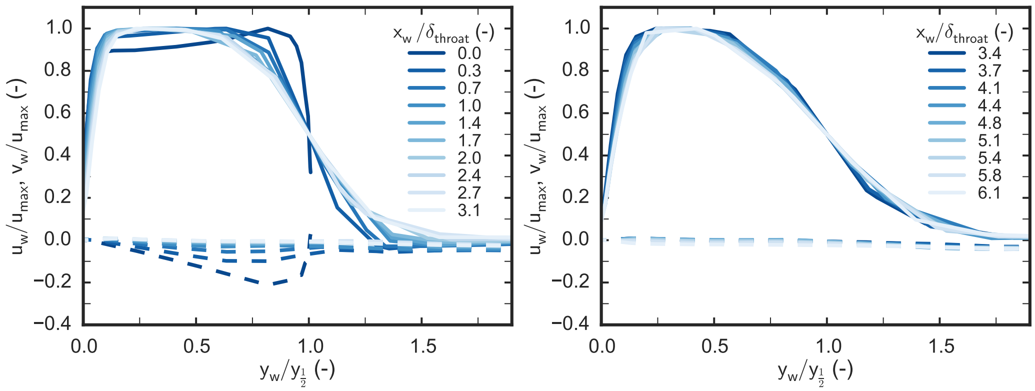

(a) upstream x_w/δ_{throat}=3.1

(b) downstream x_w/δ_{throat}=3.1

Figure 14: Normalized velocity profiles in the wall jet region obtained from LES simulations of 8 mm lance height. (solid lines) velocity component parallel to wall, (dashed lines) velocity component perpendicular to the wall.

The wall jet velocity and width at the bluff body trailing edge are important as they affect the recirculation zone. Figure 15 shows the decay of the maximum jet velocity and the jet spreading rate represented by the variation of the half-width $y_{1/2}$. Increasing the lance height increases the throat opening as well. The normalized length of the wall jet in flow direction is therefore shorter for the 16 mm configuration compared to the 8 mm configuration. The jet half-width decreases for both lance heights initially and starts to increase again at x_w/δ_{throat}=3. The decay of the maximum velocity in flow direction shows an opposite trend. The difference of the velocity profiles between the two burner configurations is, however, not found to be as significant as the difference in the spreading rate.

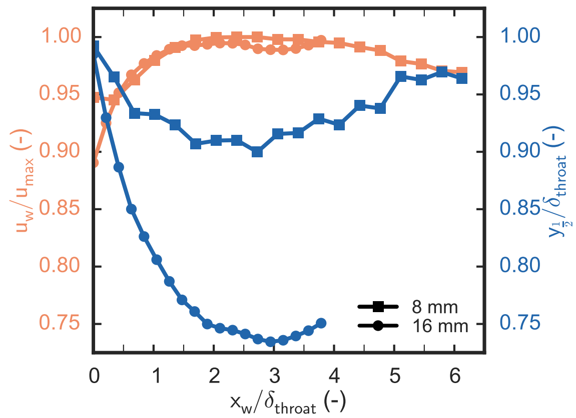

Figure 15: Decay of the maximum velocity (orange) and jet spreading rate (blue) for 8 mm lance height (squares) and 16 mm lance height (dots).

5. Discussion

The discussion is structured in three sections. Section 5.1 (turbulence model requirement) and section 5.2 (near wall treatment) discuss the requirements to the turbulence model. The latter one focuses on the two scale resolving turbulence models and their different near wall approaches only. Section 5.3 (PPBB burner flow characteristics) discusses the effect of different lance heights on the flow field, focusing mainly on regions that are likely to have a strong impact on the NO_x formation in a reacting flow. The lance height is one of the main burner parameters and its variation will affect the non-reacting and reacting configuration in a similar matter [25], which allows to draw qualitative conclusions based on the simulation of the non-reacting flow configuration.

5.1. Turbulence model requirement

All conducted RANS and URANS simulations over predicted the velocity magnitude compared to the experimental data obtained from PIV measurements. The high velocities in both the bluff body wake and recirculation zone are a consequence of the over predicted velocity in the free shear layer shedding from the bluff body trailing edge. Free shear layer flows are dominated by different instability modes depending on the type of shear layer flow (i.e., mixing layers, jets and wakes) which is challenging to accurately predict with statistical averaged models using a single set of coefficients [57]. With values for the coefficients that are appropriate to boundary-layer flows these models typically predict two-dimensional flows, as for example a plane jet, quite accurately. For axisymmetric flows with recirculation, however, effects that are not existing in two dimensional flows (such as vortex stretching) occur and can lead to large errors [58, 59].

This shortcoming of RANS turbulence models can be overcome by employing scale resolving simulations. Scale resolving simulations with an appropriate spatial and temporal resolution are able to describe the flow characteristics of the PPBB burner in good agreement with experimental data as it was seen in the simulation of the 16 mm lance height configuration. Furthermore it was shown that scale resolving simulation are superior to RANS/URANS simulations, even with a lower relative resolution as seen in the 8 mm lance height simulation. The difference in resolution between the 16 mm and the 8 mm simulation can be assessed by comparing the velocity profiles in figure 13 with the profiles given in figure 14. The lower resolution is furthermore leading to fluctuations of the normalized wall jet half-width shown in figure 15. This is, however, due to the way the half-width is obtained from a linear interpolation of the velocity profiles at the point $u_{max}/2$. Hence the resolution affects both the assessment of u_{max} as well as the linear interpolation, which magnifies the overall effect of different resolutions.

5.2. Near wall treatment

Typically it requires less effort to resolve the largest turbulence scales in free shear flows compared to wall boundary layers, where the turbulence length scale is very small compared to the boundary layer thickness. Applying LES models with under resolved wall boundary layers can, depending on the flow configuration, led to worse results than employing a suitable RANS model [23]. This motivated the development of hybrid models, such as the SBES model, where large eddies are only resolved in the free flow, while the wall boundary layer is covered by an URANS model. Hybrid models have been applied to a variety of flow problems and have been proven to outperform RANS models for many applications [60, 61, 62]. The results of the SBES simulations for both investigated lance heights confirm this general trend.

The applied LES grid resolution in the wall boundary layer was far from being sufficient to capture wall turbulence. However, LES and SBES simulation led to almost identical results. This indicates that the flow in the PPBB burner is dominated by the free shear layer flow and the flow in the recirculation zone, rather than the wall turbulence. The separation points in the flow field are clear defined by the sharp trailing edges of the bluff body and burner housing, which justifies the application of LES with under resolved wall boundary layers over a hybrid model with proper boundary layer treatment. Such a pragmatic approach has already been applied successfully by others [63]. The main advantage of hybrid models over LES is the lower computational cost due to a considerable coarser grid resolution close to walls. Running LES and hybrid simulations on the same numerical grid puts the hybrid model in the disadvantage of having to solve, typically two, additional transport equations for the turbulence quantities. Hence, in this specific case it can be beneficial to employee LES with an under resolved wall regions.

5.3. PPBB burner flow characteristics

Flow conditions in recirculation zones created by bluff bodies or swirling flow to stabilize turbulent flames (i.e., long enough residence times, high temperature and oxygen concentration) do also promote NO_x production. The recirculation zone has been identified as a major contributor to the overall NO_x formation in bluff body and swirl burners respectively [64, 65]. The NO_x formation depends on the volume of the recirculation zone, the temperature and the concentration of oxygen and nitrogen, assuming that thermal NO_x is the main contributor to the overall NO_x emission. The volume of the recirculation zone scales typically proportional to cube of the burner diameter [65]. The PIV measurements and CFD simulations of the PPBB burner showed that a variation of the lance height affected the recirculation zone length (the recirculation zone length shortened when the lance height was decreased) while the width of the recirculation zone was less affected. This indicates that the volume of the recirculation zone also correlates to the lance height, which is consequently affecting the NO_x formation in the near-burner region. The other important parameters for the NO_x formation in the near-burner region, temperature and concentrations, are depending on the dilution level [65]. Internal recirculated flue gas which is entrained into the wall jet region of the PPBB burner will therefore affect these two parameters and hence impact the NO_x formation. Quantifying this effect based on cold flow simulations is not possible. However, the axial velocity profiles along the x-coordinate at bluff body trailing edge elevation give an indication of the entrainment as function of the lance height. Numerical integration of the velocity profiles (see figures 13 and 14) showed that the wall jet in the 16 mm configuration entrains 26% less than the wall jet in the 8 mm configuration.

6. Conclusion

In the present work, non-reacting CFD simulations of the PPBB burner were conducted. Different turbulence models were investigated, ranging from steady state RANS to scale resolving simulations, in order to identify the numerical requirements for a reasonable accurate representation of the burners main flow characteristics. The results evidence the need of scale resolving simulations. RANS simulations over predicted velocity magnitude by a large margin and were hence not able to describe the flow field adequately.

Scale resolving simulations with two different turbulence models were carried out, the novel SBES model and LES simulations with the WALE subgrid model. It was found that the SBES model is able to predict the PPBB burner flow field in good agreement with experimental data. However, conducting LES simulations on the same numerical grid and hence under resolving the wall boundary layers led to almost identical results as the SBES model. For the specific case of the PPBB burner, it is therefore advantageous to use coarse LES simulations over SBES simulations in order to reduce the overall computational costs.

The dimensions of the recirculation zone downstream of the bluff body as well as the recirculating mass flow rate were quantified for two different lance heights. The results indicate that the recirculation zone volume and the recirculating mass flow rate scale proportional to the lance height. However, more burner configurations need to be studied in order to further specify the correlation between these parameters. In addition reacting flow simulations are required to quantify the affect on the NO_x emissions from the burner.

The conical wall jet configuration is a feature special to the PPBB burner and was analysed in detail. The velocity profiles in the wall jet region contain a velocity component perpendicular to the wall, which is unusual for wall jets investigated in the literature. This component decreases in flow direction and for a lance height of 8 mm a self similar flow field is starting to establish at x_w/δ_{throat}=3. The wall jet configuration allows entrainment of internally recirculated flue gas upstream of the bluff body trailing edge/flame anchor point. It was found that increasing the lance height from 8 mm to 16 mm results in a reduction of the wall jet entrainment by 26% (from 54% of the inlet mass flow to 39%) which will lead to less dilution and hence affect the overall NO_x formation. Further reacting flow simulations in a combustion chamber need to be conducted in order to quantify the degree of dilution due to the internal flue gas recirculation and the effect of a varying lance height on it.

Acknowledgement

This publication has been produced with support from the BIGCCS Centre, performed under the Norwegian research program Centres for Environment-friendly Energy Research (FME). The authors acknowledge the following partners for their contributions: Gassco, Shell, Statoil, TOTAL, ENGIE and the Research Council of Norway (193816/S60). The authors furthermore acknowledge Marcin Dutka for providing the experimental data and his assistance in interpreting it.

References

[1] K. J. Whitty, H. R. Zhang, E. G. Eddings, Emissions from Syngas Combustion, Combustion Science and Technology 180 (6) (2008) 1117–1136. doi:10.1080/00102200801963326.

[2] B. van Ruijven, D. P. van Vuuren, B. de Vries, The potential role of hydrogen in energy systems with and without climate policy, International Journal of Hydrogen Energy 32 (12) (2007) 1655–1672. doi:10.1016/j.ijhydene.2006.08.036.

[3] S. Dunn, Hydrogen futures: toward a sustainable energy system, International Journal of Hydrogen Energy 27 (3) (2002) 235–264. doi:10.1016/S0360-3199(01)00131-8.

[4] C.-C. Cormos, Evaluation of power generation schemes based on hydrogen-fueled combined cycle with carbon capture and storage (CCS), International Journal of Hydrogen Energy 36 (5) (2011) 3726–3738. doi:10.1016/j.ijhydene.2010.12.042.

[5] C.-C. Cormos, Economic implications of pre- and post-combustion calcium looping configurations applied to gasification power plants, International Journal of Hydrogen Energy 39 (20) (2014) 10507–10516. doi:10.1016/j.ijhydene.2014.05.033.

[6] M. Ditaranto, H. Li, T. Løvås, Concept of hydrogen fired gas turbine cycle with exhaust gas recirculation: Assessment of combustion and emissions performance, International Journal of Greenhouse Gas Control 37 (2015) 377–383. doi:10.1016/j.ijggc.2015.04.004.

[7] C. Baukal, R. E. Schwartz, The John Zink Combustion Handbook, 1st Edition, CRC Press LLC, 2001.

[8] D. E. Giles, S. Som, S. K. Aggarwal, NOx emission characteristics of counterflow syngas diffusion flames with airstream dilution, Fuel 85 (12-13) (2006) 1729–1742. doi:10.1016/j.fuel.2006.01.027.

[9] T. Lieuwen, V. McDonell, D. Santavicca, T. Sattelmayer, Burner Development and Operability Issues Associated with Steady Flowing Syngas Fired Combustors, Combustion Science and Technology 180 (6) (2008) 1169–1192. doi:10.1080/00102200801963375.

[10] N. A. Samiran, J.-H. Ng, M. N. Mohd Jaafar, A. Valera-Medina, C. T. Chong, H2-rich syngas strategy to reduce NOx and CO emissions and improve stability limits under premixed swirl combustion mode, International Journal of Hydrogen Energy 41 (42) (2016) 19243–19255. doi:10.1016/j.ijhydene.2016.08.095.

[11] U.S. Environmental Protection Agency, Alternative Control Techniques Document NOx Emissions from Process Heaters (Revised), Tech. rep., U.S. Environmental Protection Agency, Emission Standards Division (1993).

[12] T. Lieuwen, V. McDonell, E. Petersen, D. Santavicca, Fuel Flexibility Influences on Premixed Combustor Blowout, Flashback, Autoignition, and Stability, Journal of Engineering for Gas Turbines and Power 130 (1) (2008) 011506. doi:10.1115/1.2771243.

[13] D. R. Noble, Q. Zhang, A. Shareef, J. Tootle, A. Meyers, T. Lieuwen, Syngas Mixture Composition Effects upon Flashback and Blowout, in: Proceedings of ASME Turbo Expo, Barcelona, Spain, 2006, pp. 1–12.

[14] Q. Zhang, D. R. Noble, T. Lieuwen, Characterization of Fuel Composition Effects in H2/CO/CH4 Mixtures Upon Lean Blowout, Journal of Engineering for Gas Turbines and Power 129 (3) (2007) 688. doi:10.1115/1.2718566.

[15] Q. Zhang, D. R. Noble, S. J. Shanbhogue, T. Lieuwen, PIV Measurements in H2/CH4 Swirling Flames under near Blowoff Conditions.

[16] R. W. Schefer, Hydrogen enrichment for improved lean stability, International Journal of Hydrogen Energy 28 (2003) 1131–1141.

[17] B. Dam, G. Corona, M. Hayder, A. Choudhuri, Effects of syngas composition on combustion induced vortex breakdown (CIVB) flashback in a swirl stabilized combustor, Fuel 90 (2011) 3274–3284. doi:10.1016/j.fuel.2011.06.024.

[18] J. Fritz, M. Kröner, T. Sattelmayer, Flashback in a Swirl Burner With Cylindrical Premixing Zone, Journal of Engineering for Gas Turbines and Power 126 (2) (2004) 276. doi:10.1115/1.1473155.

[19] M. Kröner, J. Fritz, T. Sattelmayer, Flashback Limits for Combustion Induced Vortex Breakdown in a Swirl Burner, Journal of Engineering for Gas Turbines and Power 125 (3) (2003) 693. doi:10.1115/1.1582498.

[20] Ø. Spangelo, O. Sonju, T. Slungaard, M. Ditaranto, US 20090220899 A1 (2009).

[21] M. Dutka, M. Ditaranto, T. Løvås, Application of a Central Composite Design for the Study of NOx Emission Performance of a Low NOx Burner, Energies 8 (5) (2015) 3606–3627. doi:10.3390/en8053606.

[22] M. Dutka, M. Ditaranto, T. Løvås, Emission characteristics of a novel low NO x burner fueled by hydrogen-rich mixtures with methane, Journal of Power Technologies 95 (2) (2015) 105–111.

[23] F. R. Menter, Best Practice : Scale - Resolving Simulations in ANSYS CFD, Tech. Rep. 2.00 (2015).

[24] F. R. Menter, Stress-Blended Eddy Simulation (SBES) - A new Paradigm in hybrid RANS-LES Modeling, in: 6th Symposium on Hybrid RANS-LES Methods, Strasbourg, France, 2016, pp. 1–17.

[25] M. Dutka, M. Ditaranto, T. Løvås, NOx emissions and turbulent flow field in a partially premixed bluff body burner with CH4 and H2 fuels, International Journal of Hydrogen Energy 41 (28) (2016) 12397–12410. doi:10.1016/j.ijhydene.2016.05.154.

[26] M. Dutka, M. Ditaranto, T. Løvås, Investigations of air flow behavior past a conical bluff body using particle imaging velocimetry, Experiments in Fluids 56 (11) (2015) 199. doi:10.1007/s00348-015-2068-6.

[27] S. Plee, A. Mellor, Review of flashback reported in prevaporizing/premixing combustors, Combustion and Flame 32 (1978) 193–203. doi:10.1016/0010-2180(78)90093-7.

[28] A. A. Putnam, R. A. Jensen, Application of dimensionless numbers to flash-back and other combustion phenomena, Symposium on Combustion and Flame, and Explosion Phenomena 3 (1) (1948) 89–98. doi:10.1016/S1062-2896(49)80011-0.

[29] K. Wohl, Quenching, flash-back, blow-off-theory and experiment, Symposium (International) on Combustion 4 (1) (1953) 68–89. doi:10.1016/S0082-0784(53)80011-1.

[30] B. Lewis, G. Von Elbe, Combustion, flames, and explosions of gases, Academic Press, 1987.

[31] D. Davu, R. Franco, A. Choudhuri, R. Lewis, Investigation on Flashback Propensity of Syngas Premixed Flames, in: 41st AIAA/ASME/SAE/ASEE Joint Propulsion Conference & Exhibit, American Institute of Aeronautics and Astronautics, Reston, Virigina, 2005. doi:10.2514/6.2005-3585.

[32] C. Mayer, J. Sangl, T. Sattelmayer, T. Lachaux, S. Bernero, Study on the Operational Window of a Swirl Stabilized Syngas Burner Under At-

mospheric and High Pressure Conditions, Journal of Engineering for Gas Turbines and Power 134 (3) (2012) 031506. doi:10.1115/1.4004255.

[33] Y.-C. Lin, S. Daniele, P. Jansohn, K. Boulouchos, Turbulent Flame Speed as an Indicator for Flashback Propensity of Hydrogen-Rich Fuel Gases, Journal of Engineering for Gas Turbines and Power 135 (11) (2013) 111503. doi:10.1115/1.4025068.

[34] J. Kariuki, A. Dowlut, R. Yuan, R. Balachandran, E. Mastorakos, Heat release imaging in turbulent premixed methane-air flames close to blow-off, Proceedings of the Combustion Institute 35 (2015) 1443–1450. doi:10.1016/j.proci.2014.05.144.

[35] J. Kariuki, J. R. Dawson, E. Mastorakos, Measurements in turbulent premixed bluff body flames close to blow-off, Combustion and Flame 159 (8) (2012) 2589–2607. doi:10.1016/j.combustflame.2012.01.005.

[36] A. Andreini, C. Bianchini, A. Innocenti, Large Eddy Simulation of a Bluff Body Stabilized Lean Premixed Flame, Journal of Combustion 2014 (2014) 1–18. doi:10.1155/2014/710254.

[37] J. Dawson, R. Gordon, J. Kariuki, E. Mastorakos, A. Masri, M. Juddoo, Visualization of blow-off events in bluff-body stabilized turbulent premixed flames, Proceedings of the Combustion Institute 33 (1) (2011) 1559–1566. doi:10.1016/j.proci.2010.05.044.

[38] R. N. Sharma, Experimental Investigation of Conical Wall Jets, AIAA Journal 19 (1) (1981) 28–33. doi:10.2514/3.7746.

[39] R. Sharma, S. Patankar, Numerical computations of wall-jet flows, International Journal of Heat and Mass Transfer 25 (11) (1982) 1709–1718. doi:10.1016/0017-9310(82)90150-8.

[40] V. Kolár, P. Filip, A. G. Curev, Similarity prediction of wall jets on bodies of revolution, Acta Mechanica 76 (3-4) (1989) 253–263. doi:10.1007/BF01253584.

[41] T. Barth, D. Jespersen, The design and application of upwind schemes on unstructured meshes, in: 27th Aerospace Sciences Meeting, American Institute of Aeronautics and Astronautics, Reston, Virigina, 1989. doi:10.2514/6.1989-366.

[42] B. Leonard, The ULTIMATE conservative difference scheme applied to unsteady one-dimensional advection, Computer Methods in Applied Mechanics and Engineering 88 (1) (1991) 17–74. doi:10.1016/0045-7825(91)90232-U.

[43] J. P. Van Doormaal, G. D. Raithby, Enhancements of the SIMPLE method for predicting incompressible fluid flows, Numerical Heat Transfer 7 (2) (1984) 147–163. doi:10.1080/01495728408961817.

[44] S. Armfield, R. Street, The Fractional-Step Method for the Navier-Stokes Equations on Staggered Grids: The Accuracy of Three Variations, Journal of Computational Physics 153 (2) (1999) 660–665. doi:10.1006/jcph.1999.6275.

[45] J. K. Dukowicz, A. S. Dvinsky, Approximate factorization as a high order splitting for the implicit incompressible flow equations, Jour-

nal of Computational Physics 102 (2) (1992) 336–347. doi:10.1016/0021-9991(92)90376-A.

[46] J. B. Bell, P. Colella, H. M. Glaz, A second-order projection method for the incompressible navier-stokes equations, Journal of Computational Physics 85 (2) (1989) 257–283. doi:10.1016/0021-9991(89)90151-4.

[47] J. Perot, An Analysis of the Fractional Step Method, Journal of Computational Physics 108 (1) (1993) 51–58. doi:10.1006/jcph.1993.1162.

[48] B. R. Hutchinson, G. D. Raithby, A multigrid method based on the additive correction strategy, Numerical Heat Transfer 9 (5) (1986) 511–537. doi:10.1080/10407788608913491.

[49] W. Anderson, D. L. Bonhaus, An implicit upwind algorithm for computing turbulent flows on unstructured grids, Computers & Fluids 23 (1) (1994) 1–21. doi:10.1016/0045-7930(94)90023-X.

[50] M. Dutka, Emissions of nitrogen oxides from partially premixed flames stabilized on a conical bluff body, Ph.D. thesis, NTNU (2015).

[51] B. Launder, B. D. Spalding, Lectures in Mathematical Models of Turbulence, Academic Press Inc, London, England, 1972.

[52] T.-H. Shih, W. W. Liou, A. Shabbir, Z. Yang, J. Zhu, A new k- eddy viscosity model for high Reynolds number turbulent flows, Compurers Fluids 24 (3) (1995) 227–238. doi:/10.1016/0045-7930(94)00032-T.

[53] F. R. Menter, Two-equation eddy-viscosity turbulence models for en-

gineering applications, AIAA Journal 32 (8) (1994) 1598–1605. doi:10.2514/3.12149.

[54] F. Nicoud, F. Ducros, Subgrid-Scale Stress Modelling Based on the Square of the Velocity Gradient Tensor, Flow, Turbulence and Combustion 62 (3) (1999) 183–200. doi:10.1023/A:1009995426001.

[55] A. M. K. P. Taylor, J. H. Whitelaw, Velocity characteristics in the turbulent near wakes of confined axisymmetric bluff bodies 139 (2017) 391–416. doi:10.1017/S0022112084000410.

[56] J. C. R. Hunt, A. A. Wray, P. Moin, Eddies, streams, and convergence zones in turbulent flows, in: Center for Turbulence Research CTR-S88, 1988, pp. 193–208.

[57] D. A. Yoder, J. R. Debonis, N. J. Georgiadis, Modeling of Turbulent Free Shear Flows, Fluid Dynamics Conference and Exhibit 43. doi:https://doi.org/10.2514/6.2013-2721.

[58] S. B. Pope, J. H. Whitelaw, The calculation of near-wake flows, Journal of Fluid Mechanics 73 (01) (1976) 9. doi:10.1017/S0022112076001213.

[59] S. B. Pope, An explanation of the turbulent round-jet/plane-jet anomaly, AIAA Journal 16 (3) (1978) 279–281. doi:10.2514/3.7521.

[60] F. R. Menter, M. Kuntz, R. Langtry, Ten Years of Industrial Experience with the SST Turbulence Model, in: Proceedings of the 4th International Symposium on Turbulence, Heat and Mass Transfer, Vol. 4, Begell House Inc., 2003, pp. 625–632.

[61] A. Widenhorn, B. Noll, M. Aigner, Numerical Study of a Non-Reacting Turbulent Flow in a Gas-turbine Model Combustor, in: 47th AIAA Aerospace Sciences Meeting including The New Horizons Forum and Aerospace Exposition, American Institute of Aeronautics and Astronautics, Reston, Virigina, 2009. doi:10.2514/6.2009-647.

[62] F. R. Menter, Y. Egorov, The Scale-Adaptive Simulation Method for Unsteady Turbulent Flow Predictions. Part 1: Theory and Model Description, Flow, Turbulence and Combustion 85 (1) (2010) 113–138. doi:10.1007/s10494-010-9264-5.

[63] B. Farcy, L. Vervisch, P. Domingo, Large eddy simulation of selective non-catalytic reduction (SNCR): A downsizing procedure for simulating nitric-oxide reduction units, Chemical Engineering Science 139 (2015) 285–303. doi:10.1016/j.ces.2015.10.002.

[64] B. Dally, A. Masri, R. Barlow, G. Fiechtner, D. Fletcher, Measurements of no in turbulent non-premixed flames stabilized on a bluff body, Symposium (International) on Combustion 26 (2) (1996) 2191–2197. doi:10.1016/S0082-0784(96)80045-2.

[65] T.-C. Hsieh, W. J. Dahm, J. F. Driscoll, Scaling Laws for NOx Emission Performance of Burners and Furnaces from 30 kW to 12 MW, Combustion and Flame 114 (1-2) (1998) 54–80. doi:10.1016/S0010-2180(97)00289-7.